Richard Altendorfer Daniel E. Koditschek

Department of Electrical Engineering and Computer Science University of Michigan Ann Arbor, MI 48109, USA

Philip Holmes

Department of Mechanical and Aerospace Engineering Princeton University Princeton, NJ 08544, USA

Stability Analysis of a Clock-Driven Rigid-Body SLIP Model for RHex

Abstract

We apply the stability analysis for hybrid legged locomotion systems, introduced in our companion paper in this issue, to a new simple clock-driven SLIP model inspired by the robot RHex. We adopt in stance phase the three-degrees-of-freedom (3DoF) spring loaded inverted pendulum (SLIP) model introduced in our companion paper to capture RHex's pitching dynamics in the sagittal plane. The coordinating influence of RHex's open-loop clock controller is subsumed into a leg placement strategy derived from a bipedal abstraction of RHex. The "symmetric" factorization analysis introduced in our companion paper yields a necessary condition for gait stability expressed in closed form, which can be imposed directly on the clock parameter space. This represents the first reported analytical insight into how a dynamical runner might be stabilized by a completely feedforward rhythmic limb coordination pattern. Correspondence in steady-state gait location and stability characteristics with an appropriately tuned 24DoF model of RHex provides numerical evidence that the 3DoF SLIP model offers a descriptive explanation for the robot's empirical running behavior.

KEY WORDS—legged locomotion, return map, spring loaded inverted pendulum, stability

1. Introduction

In this paper we explore the applicability of the symmetry-factored stability analysis introduced in Altendorfer, Koditschek, and Holmes (2004) to the design and implementation of physically interesting running robots such as RHex (Saranli, Buehler, and Koditschek 2001). Powered by only six actuators, located at the "hips" to drive each of its six passively compliant legs, in the manner of single-spoked

The International Journal of Robotics Research Vol. 23, No. 10–11, October–November 2004, pp. 1001-1012, DOI: 10.1177/0278364904047390 ©2004 Sage Publications

rimless wheels (compare with McGeer 1990; Coleman, Chatterjee, and Ruina 1997), RHex's locomotion is driven by a single periodic "clock" signal split into phase and antiphase copies for coordinating its alternating tripod gait. A simple PD controller at each hip motor in a given tripod forces its leg to track the alternately fast and slow clock reference signals corresponding to presumed stance and swing phases. Experimentally, RHex's performance at various speeds over various terrains is strongly dependent upon the particular values of the clock parameters, and, as is typical within the feedforward control paradigm, each new situation demands its own carefully tuned parameter set (Weingarten et al. 2004). Better analytical understanding of the relationship between clock signal and steady-state gait should dramatically simplify the frequently lengthy empirical parameter tuning exercises presently required to achieve high-performance gaits (Weingarten et al. 2004).

1.1. RHex and the "Simply-Stabilized" Pogo Stick

A complete account of the relationship between RHex's internal clock signal and mechanical gait in even the simplest case would entail insight into the steady-state properties of an underactuated high degree-of-freedom (DoF) hybrid mechanical system whose Lagrangian dynamics switches among a set of 26 possible holonomically constrained models depending upon which feet are in contact with the ground. Fortunately, a growing body of numerical and empirical evidence (Altendorfer et al. 2001a) suggests that RHex, when properly tuned, exhibits in stance phase sagittal plane behavior well approximated by the spring loaded inverted pendulum (SLIP) depicted in Figure 1. Intuition suggests that the control of a pogo stick like the SLIP would require full state feedback. However, RHex, running in the open-loop mode described above, consistently exhibits a rapid return to its steady-state gait pattern during runs with long aerial phases even in the presence of significant ground perturbations (Saranli, Buehler, and Koditschek 2001; Weingarten et al. 2004).

On the other hand, there is recent numerical evidence (Seyfarth et al. 2002) and analytical proof (Ghigliazza et al. 2003) that the SLIP dynamics actually does enjoy a "simplystabilized" regime of operation. However, the apparent freedom from explicit state feedback of that 2DoF SLIP model and its variations (Seyfarth and Geyer 2002; Seyfarth, Geyer, and Herr 2003) masks implementation details that would require inertial frame sensors that RHex does not possess. In contrast, the analysis in Altendorfer, Koditschek, and Holmes (2004) allows the possibility that a purely mechanical effect might confer asymptotic stability in the 3DoF model of Figure 1 by admitting stabilization via purely body frame sensing. However, could the open-loop RHex clock coordinate a stabilizing mechanical effect? In this paper, we show analytically that the answer is "yes" in the case of a slightly abstracted version of the clock applied to a 3DoF SLIP model designed to capture RHex's pitching dynamics as well as its center of mass (COM) trajectories. We also present numerical evidence to suggest by the close correspondence of COM and pitching dynamics that this may also explain the nature of the openloop stability mechanism in RHex.

We compare the performance of the SLIP model with a 24DoF numerical surrogate for RHex, both driven with the same RHex clock parameter settings. Lacking formal results bearing on this issue, we find it useful to introduce terminology summarizing the following intuitive distinction. We will say that the correspondence is "descriptive", since the salient properties observed in the complex model are also observed in the template model fitted to it. We mean to distinguish this outcome from a stronger "prescriptive" form of correspondence where the controller design parameters (the clock settings) of the template model predict in detail the behavior of the complex model with the same design parameters.

1.2. Contributions of this Paper

The stability analysis for SLIP models using a symmetry-factored return map R as introduced in Altendorfer, Koditschek, and Holmes (2004) allows a closed-form expression for the determinant of the return map's Jacobian at a symmetric fixed point (to be explained in Section 1.3.2). This closed-form expression yields a necessary condition for asymptotic stability and a sufficient condition for instability despite the non-integrability of the SLIP dynamics. The central contributions of this paper arising from that result are the following:

 a new 3DoF SLIP model based upon the RHex gait generator (Saranli, Buehler, and Koditschek 2001; see Section 2.1) and a procedure for fitting it (Appendix A) to a previously developed 24DoF "RHex-like" numerical model (programmed in SimSect; Saranli 2000) that continues to represent the most accurate currently avail-

- able simulation of the physical RHex robot (Saranli 2002);
- application of our factored stability analysis (Altendorfer, Koditschek, and Holmes 2004) to the 3DoF SLIP model yielding for the first time analytical conditions on the rhythmic excitation pattern necessary for the stability (and sufficient for instability) of a pseudo-clock-controlled dynamical runner (Section 2.2);
- 3. a preliminary numerical study in Section 3 suggesting that our 3DoF SLIP model is a reasonably descriptive model of the RHex-like 24 DoF model programmed in SimSect (Saranli 2000).

In the remainder of this section the SLIP model with its modeling assumptions is introduced and its discrete time behavior formalized. In Section 2 the factored stability analysis of Altendorfer, Koditschek, and Holmes (2004) is applied to a new instance of the 3DoF SLIP model endowed with a RHexlike coordinating clock. The descriptive correspondence of this 3DoF SLIP model with a 24DoF model of RHex is established by a numerical study in Section 3. We close with some brief concluding remarks in Section 4.

1.3. SLIP Dynamics

1.3.1. Modeling Assumptions

In this section we establish the specifics of the SLIP models considered in this paper. They are listed in terms of the categories: geometry, trajectories, control, and potential forces.

Geometry. The 3DoF sagittal plane SLIP model is shown in Figure 1. It shows a rigid body of mass \tilde{m} and moment of inertia \tilde{I} with a massless springy leg with rest length $\tilde{\zeta}_0$ attached at a hip joint that coincides with the COM. The strength of gravity is \tilde{g} . The approximation of a leg with zero mass avoids impact losses at touchdown and simplifies the control. For convenience, all of the following expressions are formulated in dimensionless quantities, i.e.,

$$t = \tilde{t}\sqrt{\frac{\tilde{g}}{\tilde{\zeta}_0}}, \qquad y = \frac{\tilde{y}}{\tilde{\zeta}_0}, \qquad \dot{y} = \frac{\dot{\tilde{y}}}{\sqrt{\tilde{\zeta}_0\tilde{g}}},$$

$$z = \frac{\tilde{z}}{\tilde{\zeta}_0}, \qquad \dot{z} = \frac{\dot{\tilde{z}}}{\sqrt{\tilde{\zeta}_0 \tilde{g}}}, \qquad \theta = \tilde{\theta},$$

$$\dot{ heta}=\dot{ ilde{ heta}}\sqrt{\dfrac{ ilde{\zeta}}{ ilde{g}}} \qquad ext{and} \qquad I=\dfrac{ ilde{I}}{ ilde{m} ilde{\zeta}_0^2}.$$

Also shown are the pitch angle θ with respect to the horizontal and the parametrization of the COM in terms of Cartesian

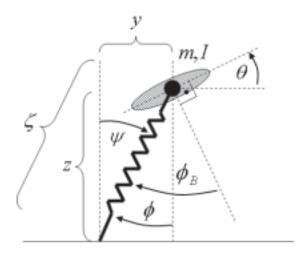


Fig. 1. Coordinate convention of SLIP with pitching dynamics. In the text, the COM coordinates are parametrized by Cartesian coordinates, i.e., $y = \zeta \sin(\psi)$ and $z = \zeta \cos(\psi)$. In flight, the leg angle ϕ is, in general, a function of time and of the SLIP's liftoff state: $\phi(t, x_0)$. The figure is taken from Altendorfer, Koditschek, and Holmes (2004).

(y, z) and polar $(\zeta = \sqrt{y^2 + z^2}, \psi = \arctan(y/z))$ coordinates with the coordinate origin at the foothold. The body is assumed to remain in the sagittal plane and its configuration is parametrized by coordinates (y, z, θ) or (ζ, ψ, θ) .

Trajectories. A full stride consists of a stance and a flight phase: in stance, we assume the foothold is fixed, the leg compressed and the body moves in the positive y direction $\dot{y} > 0$; in flight, the body describes a ballistic trajectory under the sole influence of gravity. In both phases, we choose the same parametrization of the configuration space with phase space elements denoted by $\hat{x} = (y, z, \theta, \dot{y}, \dot{z}, \dot{\theta})^{\top} \in \hat{\mathcal{X}}$. The stance phase starts with the leg uncompressed and ends when the leg has reached its rest length $\dot{\zeta}$ again. Then the flight phase begins and ends when the massless leg (appropriately placed) touches the ground. This is parametrized by a threshold function h_2 (for a general definition of threshold functions, see Altendorfer, Koditschek, and Holmes 2004) which becomes zero when the toe touches the ground:

$$h_2(\widehat{x}_0, t) = z(t) - \cos(\phi(t, \widehat{x}_0)). \tag{1}$$

If ϕ depends on \widehat{x}_0 (the liftoff state), feedback control is employed. The design of the function ϕ constitutes the control authority in our SLIP model. Stability investigations in this paper are confined to trajectories that are in the vicinity of symmetric trajectories in both stance and flight, where, for example, the liftoff and touchdown vertical heights are equal.

Control. No continuous control is exerted during stance and flight; the corresponding vector fields do not change from

stride to stride. The only control authority consists in determining the transitions between flight and stance by specifying the stance and flight time. The stance time is implicitly determined by requiring the leg to undergo a compression–decompression cycle; hence, the only designable control authority consists in specifying the flight time, which can be implicitly parametrized by the free leg angle trajectory $\phi(t, x_0)$ where x_0 denotes the SLIP COM coordinates at liftoff. Due to the massless assumption, the leg can be arbitrarily placed during flight at no energetic cost.

Potential forces.

- **P1** The potential energy is given by $E_p = z + V(y, z, \theta)$.
- **P2** The non-gravitational potential V is analytic and satisfies the symmetry relation $V(y, z, \theta) = V(-y, z, -\theta)$. This condition does not seem to severely restrict our choice of potentials.
- **P3** V factorizes as $V(y, z, \theta) = V_r(\zeta)V_p(y, z, \theta)$ with $V_r(1) = 0$. This ensures that V is zero at touchdown and liftoff. Because of the masslessness of the leg, V remains zero during flight.

1.3.2. Discrete Time Behavior of SLIP Locomotion: Return Map, and Stability

The stability properties of the SLIP hybrid dynamical systems can be assessed by a return map R acting on a (reduced) Poincaré section \mathcal{X} :

$$R: \mathcal{X} \to \mathcal{X}.$$
 (2)

The iterates of this return map *R*—the function relating the body state at a periodically (at each stride) occurring event—summarize all properties relevant to the goal of translating the body COM.

A SLIP stride consists of stance and flight, therefore its return map can be factorized as $R = R_2 \circ R_1$. The end of flight is characterized by the touchdown event, detected by the threshold equation (1). However, as detailed in Altendorfer, Koditschek, and Holmes (2004) the dynamics on $\widehat{\mathcal{X}}$ is not periodic (y(t) is monotonically increasing for trajectories as defined in Section 1.3.1). Furthermore, by conservation of total energy, the \dot{y} component of $\widehat{\mathcal{X}}$ is not independent of the other components of \widehat{x} . Therefore, the SLIP's return map is taken to act on a reduced Poincaré section \mathcal{X} with $x \in \mathcal{X}$ being the projection of \widehat{x} onto its "non-y, \dot{y} " components: $\Pi:\widehat{\mathcal{X}}\to\mathcal{X}; \quad \widehat{x}\mapsto x=(z,\theta,\dot{z},\dot{\theta})^{\top}$.

Stability of R at a symmetric fixed point $\bar{x} \in \mathcal{X}$, i.e., a fixed point of R that is also a fixed point of R_1 and R_2 , can be assessed by the location of the eigenvalues of $D_x R(\bar{x})$. If all eigenvalues lie within the unit circle, \bar{x} is a locally attracting fixed point of R. While explicit expressions for these eigenvalues are not known, a judicious use of a time reversal

symmetry G of the equations of motion of the stance and flight dynamics $G: x \mapsto (z, -\theta, -\dot{z}, \dot{\theta})^{\top}$ allows an explicit, exact expression of $|\det(D_x R(\bar{x}))|$ in terms of the control authority in the SLIP model, the leg angle trajectory $\phi(t, x_0)$, as shown in Altendorfer, Koditschek, and Holmes (2004):

$$\begin{aligned} |\det(D_{x}R(\bar{x}))| &= |1+ \\ &\frac{-\sqrt{1-z_{0}^{2}}\left(\partial_{\dot{z}_{0}}-\dot{z}_{0}\partial_{z_{0}}-\dot{\theta}_{0}\partial_{\theta_{0}}\right)\phi(t,x_{0})+\dot{z}_{0}}{-\sqrt{1-z_{0}^{2}}\partial_{t}\phi(t,x_{0})-\dot{z}_{0}} \bigg|_{\substack{t=-2\hat{z}\\x_{0}=G(\bar{x})}} \end{aligned} . \tag{3}$$

A necessary condition for local asymptotic stability of R at \bar{x} is therefore $|\det(D_x R(\bar{x}))| < 1$, whereas a sufficient condition for local asymptotic instability is $|\det(D_x R(\bar{x}))| > 1$.

1.3.3. Notation

The salient symbols used in this paper are next listed, with brief explanations of their meanings.

SLIP system definitions

 $\widehat{\mathcal{X}}_{\alpha}$ phase space

 t, \hat{x} time, phase space element (dimensionless)

 h_{α} threshold function

 \mathcal{X} reduced Poincaré section

 R_1 , R_2 return map factors on \mathcal{X}

R return map

 Π projector from $\widehat{\mathcal{X}}$ to \mathcal{X}

V conservative SLIP potential without gravity

C output map

In general, an element or a map without the diacritic $\widehat{\cdot}$ denotes an element of the reduced Poincaré section $\mathcal X$ or a map on $\mathcal X$.

1.4. Control and Sensor Modeling

In SLIP models, control is parametrized by the leg angle trajectory $\phi(t, x_0)$. The feedback loop is completed by the state vector x_0 taken at the leg liftoff event. In Altendorfer, Koditschek, and Holmes (2004) the sensory "cost" of control was assessed by the "quality" of the sensed states used in feedback. There, "quality" referred to the frame of reference of the feedback variables, since sensors implemented in the body frame are generally easier to instrument than inertial sensing. This criterion was addressed in Altendorfer, Koditschek, and Holmes (2004) by rewriting the leg angular trajectory ϕ that is defined in an inertial frame (see Figure 1) as

$$\phi(t, x_0) = \phi_C(t, C(x_0)) - \theta(t), \tag{4}$$

where C is the output map of the SLIP's discrete dynamical system and the second term in eq. (4) indicates that ϕ_C is specified with respect to the SLIP's body frame.

A leg angle trajectory that only uses sensing with respect to the body reference frame, can be modeled by the following output map C_B :

$$\begin{pmatrix} \phi_{B_0} \\ \dot{\phi}_{B_0} \end{pmatrix} = \begin{pmatrix} \arccos(z_0) + \theta_0 \\ -\frac{\dot{z}_0}{\sqrt{1 - z_0^2}} + \dot{\theta}_0 \end{pmatrix} = C_B(x_0)$$
 (5)

where ϕ_{B0} is the leg liftoff angle with respect to the body normal (see Figure 1) and $\dot{\phi}_{B0}$ is the leg's angular velocity at liftoff measured in the body frame. Specifying this trajectory in the body frame yields

$$\phi(t, x_0) = \phi_{C_R}(t, \phi_{B_0}, \dot{\phi}_{B_0}) - \theta(t). \tag{6}$$

In summary, the 3DoF SLIP model allows the distinction of the "quality" of sensing required for a particular control input, which in turn enables an assessment of the "cost" of control.

2. An RHex-Like 3DoF SLIP Model

In this section, we investigate a leg placement strategy for the control of the 3DoF SLIP model. Its importance lies in the fact that this leg placement strategy is modeled after the open-loop controller employed in RHex (Saranli, Buehler, and Koditschek 2001) within the limitations of the 3DoF SLIP model.

2.1. A Leg Angle Trajectory Based on RHex's Clock Controller

The angular reference trajectories prescribed by RHex's openloop clock controller (Saranli, Buehler, and Koditschek 2001) are specified by the (dimensionless) parameters t_c , t_s , φ_s , and φ_{off} ; see Figure 2. For one-half of the clock period t_c , the reference trajectories for the left (L) and the right (R) tripod can be expressed as functions of time in the robot's body frame (B) as

$$\phi_{B_L}(t) = \begin{cases}
\omega_s t + \varphi_{\text{off}} & 0 \le t < \frac{t_s}{2} \\
\omega_f t + \frac{\varphi_s}{2} (1 - \frac{\omega_f}{\omega_s}) + \varphi_{\text{off}} & \frac{t_s}{2} \le t < \frac{t_c}{2}
\end{cases} \tag{7}$$

$$\varphi_{B_R}(t) = \begin{cases}
-\pi + \omega_f t + \varphi_{\text{off}} & 0 \le t < \frac{t_c - t_s}{2} \\
\omega_s t - \frac{\varphi_s}{2} (1 - \frac{\omega_s}{\omega_f}) - \pi \frac{\omega_s}{\omega_f} + \varphi_{\text{off}} & \frac{t_c - t_s}{2} \le t < \frac{t_c}{2}
\end{cases}$$

where

$$\omega_s = rac{arphi_s}{t_s} < \omega_f = rac{2\pi - arphi_s}{t_c - t_s}.$$

These angular trajectories are depicted in Figure 2, and it should be understood that their values over the negative half of the clock period are prescribed so as to make them odd functions over the entire clock period.

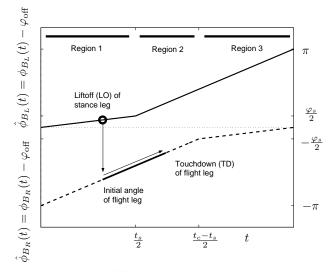


Fig. 2. Illustration of liftoff and touchdown events in the body frame of a RHex-inspired leg recirculation scheme (Saranli, Buehler, and Koditschek 2001) for SLIP with pitching dynamics.

They are enforced at each leg of the robot by a simple PD controller.

In order to implement this controller in a simplified 3DoF SLIP controller, the following assumptions are made.

- **R1** RHex's clock should prescribe motions with (substantial) flight phases, i.e., $t_s < t_c/2$.
- **R2** During stance, the effect of the stance tripod on RHex's rigid body is represented by a single (virtual) stance leg which can be approximated by a SLIP; this means that RHex's lateral motion is neglected and that the effective torque on the virtual leg that is not due to gravity can be modeled by a potential of the form **P1–P3** (see eq. (15) for the specific potential used in numerical simulations).
- R3 The PD controller that enforces the angular reference trajectories (7) during flight has infinite gains and tracks those trajectories without errors. Hence, the flight tripod can be subsumed into a single flight leg. In consequence, as the present stance leg lifts off, the PD controller can be assumed to have positioned the second (present flight) leg at the exact angle with respect to the first (present stance) leg specified by eq. (7). In contrast, during stance, the angular position and velocity variables evolve according to the SLIP stance dynamics (see Altendorfer, Koditschek, and Holmes 2004).

Assumption **R1** focuses attention on RHex's dynamical regime as opposed to the possibly quasi-static operation available to platforms with sufficiently high leg number and mitigates against stance conditions with double support that are

poorly modeled by the mechanics of Figure 1. Assumption **R2** is justified by experiments and simulation studies of RHex operating in the relevant dynamical regime (Altendorfer et al. 2001a, 2001b, 2002). Assumptions **R2** and **R3** make the controlled SLIP model a pseudo-clock controlled system, where the clock signal is turned off during stance and turned on during flight.

To develop a 3DoF SLIP model of a kind introduced in our companion paper (Altendorfer, Koditschek, and Holmes 2004), yet with a RHex-motivated leg recirculation trajectory, consider first an explicitly bipedal version.

Its kinematics is identical to that depicted in Figure 1 except that there is an additional leg. Since this additional leg is also assumed massless and stance phases where both legs touch the ground (double stance) are to be excluded by construction, the dynamics of this model will prove to be identical to the original 3DoF SLIP model defined in Section 1.3.1, as we now show. To complete the construction, we must specify the leg angle trajectories for both legs: the stance (S) and flight (F) leg. Since RHex's reference trajectories are specified with respect to the body frame, we will give expressions for the leg angle trajectories in this frame. The relation between the body and the inertial frame is given by

$$\phi_B = \phi + \theta \tag{8}$$

In the following, the left leg (L) is chosen to be the stance leg. The time t is reset to zero at the beginning of each stance and flight phase.

We model the position of the legs in stance phase as

$$\phi_{B_S}(t) = \psi(t) + \theta(t) \quad 0 < t < t_{LO}$$
 (9)

$$\phi_{B_E}(t) = \phi_{B_B} \left(\phi_{B_c}^{-1}(\phi_{B_S}(t)) \right) \quad 0 < t < t_{LO}.$$
 (10)

Here, $\psi(t)$ and $\theta(t)$ are governed by SLIP's stance phase dynamics (see Altendorfer, Koditschek, and Holmes 2004) and we effectively cancel out the independence of the flight leg by enslaving its "time" to that determined by the stance leg via eq. (10). The alternative of maintaining a true biped via the application of the second of eqs. (7) will yield a more complicated model including, for example, periods of double support whose stance phase is not described by the SLIP mechanics arising from Figure 1.

In flight, the leg angles are described by the purely kinematic equations

$$\phi_{B_S}(t) = \phi_{B_L}(t + t_{LO}) \quad 0 < t < t_{TD}
\phi_{B_F}(t) = \phi_{B_R}(\phi_{B_L}^{-1}(\phi_{B_S}(t))) \quad 0 < t < t_{TD}$$
(11)

prescribed by RHex's clock (7). The flight phase ends when the flight leg with leg angle $\phi_{B_F}(t)$ touches the ground. At the start of the next stance phase, the stance and flight legs are relabeled as flight and stance legs, respectively.

The leg angles of massless legs during flight are not governed by dynamical equations, hence the equations of motion of this bipedal SLIP version are identical to those of the

Event						
$(LO \rightarrow TD)$	$\phi(t,x_0)$	$ \det(D_x R(\bar{x})) $				
$(1 \rightarrow 1)$ $(1 \rightarrow 2)$ $(2 \rightarrow 2)$	$\omega_f t + \frac{\omega_f}{\omega_s} \left(\arccos(z_0) + \theta_0 \right) + \varphi_{\text{off}} \left(1 - \frac{\omega_f}{\omega_s} \right) - \pi - \theta(t)$ $\omega_f t + \left(\arccos(z_0) + \theta_0 \right) - \frac{\varphi_s}{2} \left(1 - \frac{\omega_f}{\omega_s} \right) - \pi - \theta(t)$	$ 1 + \frac{\frac{(-\dot{\bar{z}} - \dot{\bar{\theta}}\sqrt{1 - \bar{z}^2})(\frac{\omega_f}{\omega_s} - 1)}{(-\dot{\bar{z}} - \dot{\bar{\theta}}\sqrt{1 - \bar{z}^2}) + \omega_f \sqrt{1 - \bar{z}^2}} \overset{\dot{\bar{\theta}} < \frac{-\dot{\bar{z}}}{\sqrt{1 - \bar{z}^2}}}{>} 1$				
$(1 \rightarrow 3)$	$\omega_s t + (\arccos(z_0) + \theta_0) - \frac{\varphi_s}{2} (1 - \frac{\omega_s}{\omega_f}) - \pi \frac{\omega_s}{\omega_f} - \theta(t)$	1				
$(2 \to 3)$ $(3 \to 3)$	$\omega_s t + \frac{\omega_s}{\omega_f} \left(\arccos(z_0) + \theta_0 \right) + \varphi_{\text{off}} \left(1 - \frac{\omega_s}{\omega_f} \right) - \pi \frac{\omega_s}{\omega_f} - \theta(t)$	$ 1+\frac{(-\frac{1}{z}-\frac{1}{\theta}\sqrt{1-z^2})(\frac{\omega_s}{\omega_f}-1)}{(\frac{1}{z}-\frac{1}{\theta})(\frac{1-z^2}{\omega_f})(\frac{\omega_s}{\omega_f}-1)} < \frac{\frac{1}{\theta}<\frac{-\frac{1}{z}}{\sqrt{1-z^2}}}{1}$				

Table 1. Functional Expressions for $\phi(t, x_0)$ and $|\det(D_x R(\bar{x}))|$ for Different Locations of the Liftoff and Touchdown

monopedal SLIP model presented in Altendorfer, Koditschek, and Holmes (2004). Moreover, the end of flight is solely determined by the flight leg with leg angle $\phi_{B_F}(t)$; the flight leg during stance and the stance leg during flight can therefore be ignored. The complete expression for the effectively resulting monopedal recirculation strategy now derives from eqs. (11) and (8):

$$\phi(t, x_0) = \phi_{B_F}(t) - \theta(t) = \phi_{B_R}(t + t_{LO}) - \theta(t)$$
 (12)

where $t_{LO} = \phi_{B_L}^{-1}(\phi_0 + \theta_0)$ is the time with respect to the RHex clock when liftoff occurs and $\phi_0 = \arccos(z_0)$ is the angle of the stance leg at liftoff in the inertial frame. This procedure is illustrated within the body frame in Figure 2.

By inserting the expressions for the RHex clock trajectory (7) into eq. (12), the angular trajectory for the 3DoF SLIP system is obtained. Since the leg angle trajectory $\phi(t, x_0)$ (12) is based on two piecewise-defined functions (7), different expressions for $\phi(t, x_0)$ are derived depending on where liftoff and touchdown occurs. We distinguish three regions (see Figure 2) with respect to the RHex clock time:

region 1

$$0 \leq t < \frac{t_s}{2},$$

region 2

$$\frac{t_s}{2} \le t < \frac{t_c - t_s}{2},$$

and region 3

$$\frac{t_c-t_s}{2}\leq t<\frac{t_c}{2}.$$

We enumerate these different liftoff–touchdown combinations by two numbers (LO \rightarrow TD) which denote the region in Figure 2 where liftoff and touchdown occurs. Six different cases together with the corresponding leg angle trajectory and the absolute value of the determinant of the return map Jacobian at a fixed point are listed in Table 1. "Backward" cases

such as $(2 \rightarrow 1)$ are not listed as they would correspond to multiple revolutions of the leg which we do not consider.

Table 1 shows that the angular trajectory at any instant in time has the general form

$$\phi(t, x_0) = \omega t + k \underbrace{(\arccos(z_0) + \theta_0)}_{=\phi_{B_0}} + \alpha_A - \theta(t)$$
 (13)

with $\omega \in \{\omega_f, \omega_s\}$, and $k \in \{\omega_s/\omega_f, 1, \omega_f/\omega_s\}$; the different values of α_A can be read from Table 1. The value $|\det(D_x R(\bar{x}))| = 1$ for k = 1 is the result of an underlying time reversal symmetry of the discrete flight map as shown in appendix A of Altendorfer, Koditschek, and Holmes (2004). This opens the possibility of neutrally stable behavior of this 3DoF SLIP system analogous to the one proven for a 2DoF SLIP system in appendix C of Altendorfer, Koditschek, and Holmes (2004).

Note that eq. (13) is of the form of eq. (6) with the body frame sensor model $C_B(x_0) = \arccos(z_0) + \theta_0 = \phi_{B_0}$, i.e., no body frame velocity measurement is required. Based on the properties of symmetric orbits that we focus on in this paper, a necessary condition on a RHex clock parameter for asymptotic stability can now be derived.

2.2. A Necessary Condition for Asymptotic Stability

For symmetric orbits, the liftoff and touchdown leg angles in the inertial frame are of equal magnitude but opposite sign: $\phi_0 = -\phi(t_{TD})$. This also holds for the pitching angles: $\theta_0 = -\theta(t_{TD})$. Using eq. (8) to translate the liftoff and touchdown angles to the body frame

$$\phi_B(t_{LO}) = \phi_0 + \theta_0$$

$$\phi_B(t_{TD}) = \phi(t_{TD}) + \theta(t_{TD})$$

we obtain $\phi_B(t_{LO}) + \phi_B(t_{TD}) = 0$. With the definition $\hat{\phi}_B = \phi_B - \varphi_{\text{off}}$ as in Figure 2, this equality can be rewritten as

$$\hat{\phi}_R(t_{LO}) + \hat{\phi}_R(t_{TD}) = -2\varphi_{\text{off}}.$$
 (14)

Table 2. Table of Allowed Transitions (LO \rightarrow TD) for Symmetric Orbits in Terms of the Sign of the Leg Offset Parameter φ_{off} of the RHex Clock

, on			
$(\text{LO} \rightarrow \text{TD})$	$\varphi_{ m off} < 0$	$\varphi_{ m off}=0$	$\varphi_{ m off}>0$
$(1 \to 1)$ $(1 \to 2)$	no	no	yes
$(2 \to 2)$ $(1 \to 3)$	yes	yes	yes
$(2 \rightarrow 3)$ $(3 \rightarrow 3)$	yes	no	no

[&]quot;Backward" transitions such as $(2 \to 1)$ are not considered as they would correspond to multiple revolutions of the leg during flight.

This equation constrains the allowed liftoff–touchdown transitions between regions 1–3 in Figure 2 for symmetric orbits; e.g., $\varphi_{\rm off} > 0$ excludes transitions between the regions $(2 \to 3)$ and $(3 \to 3)$ because there we have $\hat{\varphi}_B(t_{LO}) \ge |\hat{\varphi}_B(t_{TD})|$ whereas $|\hat{\varphi}_B(t_{TD})| > \hat{\varphi}_B(t_{LO})$ by eq. (14). Table 2 shows which liftoff–touchdown transitions are possible as a function of the sign of RHex clock's leg offset angle $\varphi_{\rm off}$.

If $\dot{\bar{\theta}}<-\dot{\bar{z}}/\sqrt{1-\bar{z}^2}$, the determinant for the transitions $(2\to 3)$ and $(3\to 3)$ will be less than one. Hence, a necessary condition for asymptotic stability is $\varphi_{\rm off}<0$ provided that $\dot{\bar{\theta}}<-\dot{\bar{z}}/\sqrt{1-\bar{z}^2}$. On the other hand, a sufficient condition for instability (including neutral stability) is $\varphi_{\rm off}>0$ provided that $\dot{\bar{\theta}}<-\dot{\bar{z}}/\sqrt{1-\bar{z}^2}$.

It should be emphasized that the expressions in Table 1 are independent of the specific 3DoF SLIP potential V as long as the general conditions **P1–P3** listed in Section 1.3.1 are obeyed. However, a specific SLIP model does influence the location of fixed points \bar{x} and therefore the numerical value of the determinant for the cases $1 \rightarrow 1, 1 \rightarrow 2, 2 \rightarrow 3, 3 \rightarrow 3$ as well as the location of the eigenvalues.

This analysis provides for the first time an analytical tool to assess the stability properties of a rigid-body RHex-like SLIP model. We now examine its relevance to the SimSect model of the open-loop clock-driven robot RHex.

3. Application: Toward Hierarchical Control of a Hexapedal Robot

In this section we explore numerically the applicability of these ideas to the robot RHex (Saranli, Buehler, and Koditschek 2001). In Section 3.1 we review the general approach to hierarchical control (Full and Koditschek 1999) in the specific context of a RHex-like anchor system compared to the SLIP template with a physically motivated stance phase potential and leg angle trajectory. In Section 3.2 we present simulation results and assess the degree of correspondence between the simulated anchor and its putative template.

3.1. Control of the Anchor by Controlling the Template

We seek to assess the advantages and costs of imposing a hierarchical organization on the control and stabilization architectures of complex, high-DoF mechanisms such as RHex. In this paper, this assessment centers on exploring the notion of the template and anchor hierarchy introduced in Full and Koditschek (1999).

A template is a low-dimensional model of an abstract mechanism operating within an idealized environment capable of representing a specific task of interest. It generally must be "anchored" in some appropriate higher-dimensional physical mechanism designed to actually carry out the task in the real world. We seek controllers whose closed loops result in a "prescriptive" correspondence (defined in Section 1.1) of the dynamics of the high- and low-DoF models. Hence, the controller must (a) force the high-dimensional anchor to follow the dynamics of the low-dimensional template (anchoring), and (b) control the template to achieve a certain task. For example, Koditschek and colleagues have anchored a simple stable periodic vertical (1DoF) batting template (Buehler, Koditschek, and Kindlman 1990) to achieve a two-ball stable juggling task in planar (4DoF; Buehler, Koditschek, and Kindlman 1994) and three-dimensional (6DoF; Rizzi, Whitcomb, and Koditschek 1992) environments. In these settings, a continuous time controller is used to create within the total state space (formed by coupling the "host" physical mechanism with its task environment) an attracting invariant submanifold whose restriction dynamics is a copy of the template (Buehler and Koditschek 1990; Westervelt, Grizzle, and Koditschek 2003). In other settings (e.g., in Nakanishi, Fukuda, and Koditschek 2000), we have simply approximated the desired restriction dynamics. Recently, the SLIP template has been "approximately anchored" in a 24DoF SimSect model of RHex (Saranli 2002).

However, in all these cases, the anchoring controllers have relied on "inverse dynamics" (the exact cancellation of unwanted dynamical terms and introduction of desired dynamical terms) that requires very high bandwidth accurate state feedback as well as very accurate robot models. In the present setting, with the limitation to individual hip angles sensed with respect to the body frame, there is not enough state information to even approximate an inverse dynamics solution. Yet it is an empirical fact that the physical machine anchors some form of the SLIP template (Altendorfer et al. 2001a) that seems to persist over a wide variation in clock parameter settings (Weingarten et al. 2004). The question now arises as to how to derive proper advantage of this useful but presently poorly understood fact. Whereas the nature of the anchoring mechanism remains open, the previous section provides the beginnings of a method for commanding the behavior of the template, and hopefully thereby the salient properties of the gait of robot that anchors it. Namely, for the RHex clock parameter settings that lead to a stable steady-state gait in the physical machine it is natural to ask whether they will produce the same gait in the anchored SLIP template. Short of answering that question in the physically realistic machine, we now take a preliminary look at its resolution respecting our best numerical simulation written in SimSect (Saranli 2000).

Specifically, we provide numerical evidence for the agreement of the stability properties of an RHex-like model programmed in the SimSect simulation environment (Saranli 2000) with the stability properties of the 3DoF SLIP model introduced in Section 2.1. This numerical surrogate for the physical machine does not exactly predict RHex's empirical performance in any specific regime, but exhibits general enough correspondence to the robot's qualitative behavior that we use it regularly as a debugging tool prior to physical experiments with a new controller (Weingarten et al. 2004). We now show that in a physically interesting operational regime, stable simulations in SimSect correspond to stable fixed points of the corresponding SLIP model.

Here, "correspondence" is established by fitting simulation data to a 3DoF SLIP model with an RHex-like leg angle trajectory (13) using the RHex clock parameters of the SimSect simulation. The stance phase potential used in this model

$$V(y, z, \theta) = \frac{\gamma}{2} (\zeta - 1)^2 \left(1 + c_{\theta\theta} \theta^2 + c_{\theta\psi} \theta \psi + c_{\psi\psi} \psi^2 \right)$$
(15)

is the generalization of a potential $V(\psi, \theta) = (\gamma/2)(\zeta - 1)^2(1 + c_{\theta+\psi}(\theta + \psi)^2)$, which could be implemented in a physical single-leg hopping robot by a passive leg spring and a passive torsional spring between the body and the leg. The generalized potential (15) would require passive springs attached to a "comoving" inertial frame, preventing a physical implementation with a one-legged robot. However, we believe that this model reasonably approximates the moments due to the "outrigger" front and back legs, compressed against the horizontal ground surface, in the tripod stance phase of RHex.

3.2. Correspondence Between RHex-Like Simulations and Their Fitted SLIP Models

Simulations of an RHex-like hexapedal robot were run in Sim-Sect (Saranli 2000) over a discretized range of clock parameters of RHex's open-loop clock controller (Saranli, Buehler, and Koditschek 2001) that respect assumptions **R1**, **R2**, **R3** of Section 2.1: $t_c \in [0.235, 0.245], \varphi_s \in [0.84, 1.04], \varphi_{\text{off}} \in [-0.16, 0.04], d_f \in [0.52, 0.6],$ where the duty factor d_f is defined as $d_f = (t_c - t_s)/t_c$. Of the resulting 1815 SimSect simulations, 522 (= 29%) were stable according to the criteria of Appendix A1. Then, a 3DoF SLIP model with the stance potential (15) and the leg angle trajectory (13) was fitted to those stable cases following the fitting procedure outlined in Appendix A2.

We will show that the 3DoF SLIP model approximates the 24DoF SimSect steady-state dynamics surprisingly well, given the gulf in dimension. Specifically, the trajectory fitting errors are very small on average; the fixed points of the Sim-Sect simulations and the fitted SLIP models are within the same order of magnitude, and the asymptotic behavior agrees in almost all cases, as detailed below.

However, while the fitted SLIP models provide good correspondence once a specific SimSect operating point has been selected, it is not the case that a priori specification of clock parameters yields a SLIP model whose fixed point locus and stability predicts that observed in the SimSect model. In this sense, the present SLIP model provides a descriptive but not prescriptive representation of the SimSect dynamics.

3.2.1. Correspondence of Trajectories

The quality of the fit is assessed for each stable simulation by the two fitting error numbers Δyz_{L_2} and $\Delta\theta_{L_2}$ as described in Appendix A3. The average fitting error and standard deviation for both errors for the 522 stable SimSect simulations for the Cartesian coordinates is small $\Delta yz_{L_2}=3.82\pm0.42\%$ and of similar magnitude as the fitting errors for 2DoF SLIP models observed in Altendorfer et al. (2002), whereas the average fitting error for the pitch coordinates, $\Delta\theta_{L_2}=93.65\pm25.76\%$, is considerably larger. As an illustration of the fitting results a sample SLIP fit is presented in Figure 3. The data trajectories of y(t), $\dot{y}(t)$, z(t), $\dot{z}(t)$, $\theta(t)$, $\dot{\theta}(t)$, $\zeta(t)$ are plotted together with the trajectories of their fitted SLIP models.

The large $\Delta \theta_{L_2}$ fitting error is an indication that the proposed 3DoF SLIP model is not a sufficiently accurate abstraction of SimSect's pitching dynamics. A further contributing factor to the size of $\Delta\theta_{L_2}$ is the fact that the magnitudes of both $\theta(t)$ and $\dot{\theta}(t)$ trajectories are small, which makes the denominator of the fitting error $\Delta\theta_{L_2}$ (18) small. Another deviation of the dynamics of the fitted SLIP model from SimSect is apparent in the $\dot{y}(t)$ trajectories of Figure 3, which is typical of all fitted SLIP models. Here, the fitted SLIP trajectory is out of phase with the SimSect COM trajectory; nevertheless, the fitting error $\Delta y z_{L_2}$ is small because of the large average value of the SimSect trajectory that enters eq. (18). We believe that the acceleration in the forward direction during the leg compression phase seen in SimSect as opposed to a deceleration in the corresponding SLIP model is due to the non-conservative nature of the SimSect model, where energy is pumped into the system by the hip torques, and then lost to damping and friction (a similar discrepancy motivated the inclusion of dissipative losses and hip torques in a model of horizontal plane insect locomotion; Schmitt and Holmes 2003).

3.2.2. Correspondence of Fixed Points

Next, we investigate whether the fixed point of the fitted SLIP model accurately predicts the fixed point of the corresponding SimSect run. In general, the fitted SLIP model with the initial condition obtained from its SimSect simulation as

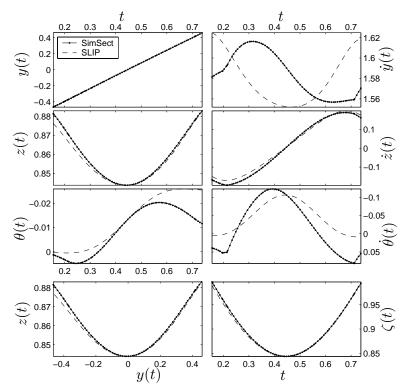


Fig. 3. Trajectories of a stable SimSect simulation and the corresponding trajectories of the fitted SLIP model. The fitting errors are $\Delta y z_{L_2} = 3.56\%$ and $\Delta \theta_{L_2} = 51.46\%$.

described in Appendix A3 will not operate at a fixed point of its return map R. Hence, a root-finding algorithm (Matlab's "fsolve") is employed to determine the fixed point \bar{x}_{SLIP} (if it exists) of the return map R of the fitted SLIP model as well as the eigenvalues $\{\lambda_i\}_{i=1,\dots,4}$ of the Jacobian of the return map: $D_x R(\bar{x}_{SLIP})$. The fixed point \bar{x}_{SLIP} is then compared to the "fixed point" \bar{x}_{Sim} , the appropriate projection of the initial data point of the SimSect simulation stance data. Scatter plots of the components of the fixed points \bar{x}_{SLIP} and \bar{x}_{Sim} of all stable SimSect simulations are shown in Figure 4. For perfect correspondence of the SimSect and SLIP dynamics, all fixed point components should lie on the 45° identity lines. The fixed point components are, in general, well correlated (correlation coefficients $\rho \geq 0.5$), except for $\dot{\bar{z}}_{SLIP}$ and $\dot{\bar{z}}_{Sim}$. The fixed points $\dot{\bar{z}}_{Sim}$ assume an almost constant value and the pitching components of \bar{x}_{SLIP} tend to be of similar magnitude but opposite sign of the pitching components of \bar{x}_{Sim} .

The correspondence in terms of the apex coordinates \bar{z}_A , the apex height, and $\dot{\bar{y}}_A$, the apex forward speed, is more persuasive (Figure 5); the scatter plots show strong correlation (correlation coefficients $\rho > 0.85$). This improvement might be due to the fact that the apex event is unambiguously defined for both SimSect and SLIP simulations, whereas only an effective touchdown event where at least one of the three stance legs touch the ground (see Section A1) can be defined

for the six-legged SimSect model. The small offset of about 3% in the apex forward speeds can be explained by the phase shifts that are generally observed in the $\dot{y}(t)$ component of the fitted SLIP with respect to the SimSect simulation data; see Figure 3.

In summary, the orders of magnitude of the components of the fixed points match well despite the simplicity of the SLIP model with respect to the robot RHex.

3.2.3. Correspondence of Stability at a Fixed Point

Given the numerically determined eigenvalues $\{\lambda_i\}_{i=1,\dots,4}$ of a fitted SLIP model at its fixed point \bar{x}_{SLIP} , its local asymptotic stability properties can be assessed. The magnitude of the determinant $|\Pi_{i=1}^4\lambda_i|$ agrees to a high numerical precision with the appropriate expression in Table 1, predicting instability for $\varphi_{\rm off}>0$ and allowing asymptotic stability for $\varphi_{\rm off}<0$ according to Table 2 (the constraint $\dot{\bar{\theta}}<-\dot{\bar{z}}/\sqrt{1-\bar{z}^2}$ was satisfied in all numerical simulations). Thus, the numerical simulation results for our 3DoF SLIP model correspond exactly to the theoretical predictions, as the analysis of Section 2 dictates. In contrast, the correspondence between the stability of the SLIP and the SimSect models is somewhat blurred by the practicalities of the purely numerical analysis available to the latter.

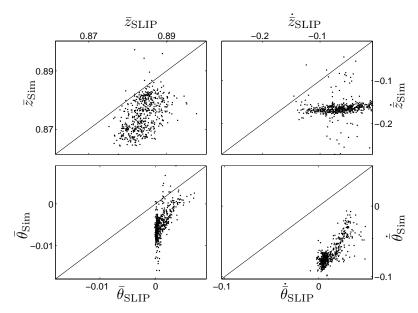


Fig. 4. Scatter plots of components of the fixed points of stable SimSect simulations versus the corresponding fixed point components of the fitted SLIP models. For perfect correspondence, all points should lie on the identity line.

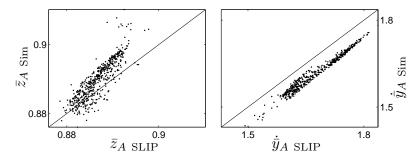


Fig. 5. Scatter plots of the apex height and apex forward velocity at fixed points of stable SimSect simulations versus the corresponding apex coordinates of the fitted SLIP models.

SimSect simulations that are stable in the sense of Appendix A1 are found with similar frequency of occurrence for $\varphi_{\rm off} > 0$ as well as for $\varphi_{\rm off} < 0$ for the range of clock parameters considered. However, this discrepancy in numerical classification does not necessarily indict the accuracy of the SLIP stability predictions since most of the unstable SLIP instances in this regime had very weak instability with eigenvalues just barely exceeding unity magnitude; for example, $|\lambda_i| < 1.05, i = 1, ..., 4$ for 92% of the 522 SimSect runs that were classified as "stable". Indeed, SLIP simulations in this regime would require many iterations to detect instability according to the numerical criteria applied to the SimSect trajectories. For example, see figure 3(b) in Altendorfer, Koditschek, and Holmes (2004) for a "weakly" unstable trajectory of a 2DoF SLIP model with $|\lambda_1| = |\lambda_2| \approx 1.007$.

Thus, the practical instability criteria of the numerical study (the first two criteria of Appendix A1) would fail to detect SLIP instability. In summary, the stability criteria of this

preliminary numerical study (appropriate to the approximate relationship between RHex's physical performance and the SimSect model) demonstrate good correspondence between SLIP and SimSect model stability properties over the regimes examined, but are insufficiently precise for a complete assessment of the quality of fit.

4. Conclusions

In this paper we apply the factored stability analysis of Altendorfer, Koditschek, and Holmes (2004) to a particular 3DoF SLIP model with pitching dynamics and an RHex-like leg recirculation strategy that satisfies the theoretically derived necessary condition for asymptotic stability in certain parameter regions.

This is the first reported use of analytical methods to help account for the stabilizing (or destabilizing) influence of RHex clock parameter settings driving any physical mechanism in an open-loop manner. We also offer preliminary results of an accompanying numerical study intended to shed light on how close this newly tractable 3DoF SLIP model may come to serving as a template for the physical robot, RHex, itself (Saranli, Buehler, and Koditschek 2001). Numerical results indicate that the SLIP model indeed captures the salient aspects of the steady-state dynamics (small Cartesian fitting errors and order of magnitude agreement of fixed points) of the SimSect model. It also accurately predicts the SimSect model's stability properties within the limitations of the finite time and finite iteration stability criteria of Appendix A1.

This example application of the symmetry factored stability analysis of Altendorfer, Koditschek, and Holmes (2004) begins to suggest the advance over solely empirical tuning (Weingarten et al. 2004) to be made by strengthening the theoretical foundations of locomotion control. It seems clear that further extensions of the theory capable of addressing the consequences of energy increasing (e.g., actuators) and decreasing (e.g., friction) influences will be required before we have a body of theory that can directly inform the design of controllers for useful physical machines like RHex.

Appendix A: SLIP Fitting Protocol

A1. SimSect Simulations

The following criteria must be met by a SimSect simulation (for a detailed discussion of the SimSect simulation environment, see Saranli 2000) that has aerial phases and that is considered stable.

- A simulation must successfully complete 10 s of simulation time without crashing, i.e., by maintaining upright forward locomotion.
- 2. A simulation must be stable over the last 20 strides. A stride is a part of the trajectory between two isolated maxima of the z-component of the COM trajectory. Stability is measured in terms of the maximal deviation of averaged linear and angular velocities at the minimum of the z-component of the COM trajectory for the last 20 individual strides with respect to the respective averaged quantities over those strides.
- 3. The second to last stride of the simulation is selected and is required to exhibit a flight phase at the two isolated maxima delimiting a stride, i.e., none of SimSect's six legs touches the ground over a finite amount of time around these maxima. In addition, at the minimum of the *z*-component of the COM trajectory all three legs of the stance tripod are required to touch the ground, whereas all three legs of the flight tripod must be off the ground.

Once a SimSect simulation has passed all of the above conditions, it is called stable. Then a 3DoF SLIP model is

fit to the simulation data of the selected stride. The simulation data required for fitting are given by time series vectors $\tilde{\boldsymbol{y}}_{Sim}$, $\dot{\tilde{\boldsymbol{y}}}_{Sim}$, $\dot{\tilde{\boldsymbol{y}}}_{Sim}$, $\dot{\tilde{\boldsymbol{z}}}_{Sim}$, $\dot{\tilde{\boldsymbol{z}}}_{Sim}$, $\dot{\tilde{\boldsymbol{z}}}_{Sim}$, $\dot{\tilde{\boldsymbol{\theta}}}_{Sim}$, $\dot{\tilde{\boldsymbol{\theta}}}_{Sim}$, which form the part of the stride trajectory where at least one of the three legs of the stance tripod of the SimSect model is on the ground whereas all three legs of the flight tripod are in the air ("stance phase"). Here, the *y*-coordinate denotes the forward position of SimSect's COM, *z* denotes the vertical position of the robot's COM, and θ denotes the pitch angle of the robot in the sagittal plane.

A2. Fitting Procedure

The equations of motion of SLIP's stance phase (see Altendorfer, Koditschek, and Holmes 2004) and the equation for the total conserved energy in terms of dimensional variables can be written as

$$\tilde{m}\ddot{\tilde{y}} = -\partial_{\tilde{y}}V(\tilde{y},\tilde{z},\tilde{\theta})$$

$$\tilde{m}(\ddot{\tilde{z}} + \tilde{g}) = -\partial_{\tilde{z}}V(\tilde{y},\tilde{z},\tilde{\theta})$$

$$\tilde{I}\ddot{\tilde{\theta}} = -\partial_{\tilde{\theta}}V(\tilde{y},\tilde{z},\tilde{\theta})$$

$$\frac{\tilde{I}}{2}\dot{\tilde{\theta}}^{2} = \tilde{E}_{0} - V(\tilde{y},\tilde{z},\tilde{\theta}) - \tilde{m}\tilde{g}\tilde{z} - \frac{\tilde{m}}{2}(\dot{\tilde{y}}^{2} + \dot{\tilde{z}}^{2})$$
(16)

with $V(\tilde{y}, \tilde{z}, \tilde{\theta}) = \frac{\tilde{\kappa}}{2} (\tilde{\zeta} - \tilde{\zeta}_0)^2 (1 + c_{\theta\theta} \tilde{\theta}^2 + c_{\theta\psi} \tilde{\theta} \tilde{\psi} + c_{\psi\psi} \tilde{\psi}^2)$, $\tilde{\zeta} = \sqrt{(\tilde{y} + \Delta \tilde{y})^2 + \tilde{z}^2}$, and $\tilde{\psi} = \arctan{(\tilde{y} + \Delta \tilde{y}/\tilde{z})}$. We want to determine the a priori unknown parameters $c_f = (\tilde{\kappa}, \tilde{\zeta}_0, c_{\theta\theta}, c_{\theta\psi}, c_{\psi\psi}, \Delta \tilde{y}, \tilde{E}_0)$ by fitting the numerical data of a single stance phase of a SimSect simulation to eqs. (16). The first five components of c_f are parameters that determine the SLIP potential V. The sixth component, $\Delta \tilde{y}$, resets the y-coordinate origin and hence determines the y-position of the foothold of the fitted virtual SLIP with respect to the stance data. The fitting parameters also include the total energy \tilde{E}_0 , because in SimSect the total energy is not constant due to damping, frictional losses and hip motor torques.

In order to determine the fitting parameters c_f a nonlinear fitting procedure (using Matlab's "lsqcurvefit") is employed that computes

$$\min_{c_f} ||F_{fit}(c_f, \tilde{x}) - \tilde{x}_{fit}||_2^2$$
 (17)

where $\tilde{\boldsymbol{x}} = (\tilde{\boldsymbol{y}}_{Sim}, \tilde{\boldsymbol{z}}_{Sim}, \tilde{\boldsymbol{\theta}}_{Sim}, \dot{\tilde{\boldsymbol{y}}}_{Sim}^2 + \dot{\tilde{\boldsymbol{z}}}_{Sim}^2)$, $\tilde{\boldsymbol{x}}_{fit} = (\tilde{m}\ddot{\tilde{\boldsymbol{y}}}_{Sim}, \tilde{m}(\ddot{\tilde{\boldsymbol{z}}}_{Sim} + g), \tilde{I}\ddot{\tilde{\boldsymbol{\theta}}}_{Sim}, (\tilde{I}/2)\dot{\tilde{\boldsymbol{\theta}}}_{Sim}^2)$, and $F_{fit}(c_f, \tilde{\boldsymbol{x}})$ is the expression obtained by inserting $\tilde{\boldsymbol{x}}$ into the right-hand side of eq. (16). Once a solution c_f has been found, the quality of the fit must be quantified.

A3. Fitting Error Assessment

Instead of using the residual (17), which lacks an intuitive physical interpretation and does not represent an error

^{1.} The stance tripod of RHex and the SimSect model is formed by those three legs that are simultaneously in the slow phase of the RHex clock controller. The flight tripod is formed by the other three legs that are in the fast phase.

measure in phase space, we compute fitting errors as in Schwind (1998) and Altendorfer et al. (2001b). The assessment of the quality of the fit proceeds in two steps. First, a SLIP simulation over the same period of time as the data trajectory is run with the fitted value of c_f . The initial conditions are taken to be the positions and velocities of the data trajectory at the minimum of $\tilde{\mathbf{z}}_{Sim}$. Secondly, the resulting SLIP trajectories $\tilde{\mathbf{y}}_{SLIP}$, $\dot{\tilde{\mathbf{y}}}_{SLIP}$, $\dot{\tilde{\mathbf{z}}}_{SLIP}$, $\dot{\tilde{\mathbf{e}}}_{SLIP}$, $\dot{\tilde{\mathbf{e}}}_{SLIP}$, are compared to the data trajectories by L_2 percent errors:

$$\Delta X_{L_2} = 100 \frac{||X_{Sim} - X_{SLIP}||_2}{||X_{Sim}||_2}.$$
 (18)

Here, $X \in \{\tilde{\mathbf{y}}, \dot{\tilde{\mathbf{y}}}, \tilde{\mathbf{z}}, \dot{\tilde{\mathbf{z}}}, \tilde{\boldsymbol{\theta}}, \dot{\tilde{\boldsymbol{\theta}}}\}$ and $||\cdot||_2$ is the standard 2-norm. In an effort to simplify the assessment of the fitting error, the quality of the fit is reported as two numbers: the average L_2 percent error of the Cartesian coordinates $\Delta y z_{L_2} = (\Delta \tilde{\mathbf{y}}_{L_2} + \Delta \dot{\tilde{\mathbf{z}}}_{L_2})/4$, and the average L_2 percent error of the pitch coordinates $\Delta \theta_{L_2} = (\Delta \tilde{\boldsymbol{\theta}}_{L_2} + \Delta \dot{\tilde{\boldsymbol{\theta}}}_{L_2})/2$.

Acknowledgments

This work is supported in part by DARPA/ONR Grant N00014-98-1-0747 and DoE grant DE-FG02-95ER25238 (PH).

References

- Altendorfer, R., Moore, N., Komsuoğlu, H., Buehler, M., Brown, H.B. Jr, McMordie, D., Saranli, U., Full, R., and Koditschek, D.E. 2001a. RHex: a biologically inspired hexapod runner. *Autonomous Robots* 11:207–213.
- Altendorfer, R., Saranli, U., Komsuoğlu, H., Koditschek, D.E., Brown, H.B. Jr, Buehler, M., Moore, N., McMordie, D., and Full, R. 2001b. Evidence for spring loaded inverted pendulum running in a hexapod robot. *Experimental Robotics VII*, Springer-Verlag, Berlin, pp. 291–302.
- Altendorfer, R., Ghigliazza, R.M., Holmes, P., and Koditschek, D.E. 2002. Exploiting passive stability for hierarchical control. *Proceedings of the 5th International Conference on Climbing and Walking Robots (CLAWAR 2002)*, Paris, France, pp. 177–184.
- Altendorfer, R., Koditschek, D.E., and Holmes, P. 2004. Stability analysis of legged locomotion models by symmetry-factored return maps. *International Journal of Robotics Research* 23(10–11):979–999.
- Buehler, M., and Koditschek, D.E. 1990. From stable to chaotic juggling: theory, simulation, and experiments. *Proceedings of the IEEE International Conference on Robotics and Automation (ICRA)*, Cincinnati, OH, pp. 1976–1981.
- Buehler, M., Koditschek, D.E., and Kindlman, P.J. 1990. A family of robot control strategies for intermittent dynamical environments. *IEEE Control Systems Magazine* 10(2):16–22.
- 2. Since total energy is not constant over a stance phase in SimSect, the \dot{y} -component of the initial conditions is scaled to the fitted total energy \tilde{E}_0 .

- Buehler, M., Koditschek, D.E., and Kindlman, P.J. 1994. Planning and control of robotic juggling and catching tasks. *International Journal of Robotics Research* 13(2):101–118.
- Coleman, M.J., Chatterjee, A., and Ruina, A. 1997. Motions of a rimless spoked wheel: a simple 3D system with impacts. *Dynamics and Stability of Systems* 5(3):139–160.
- Full, R., and Koditschek, D.E. 1999. Templates and anchors: neuromechanical hypothesis of legged locomotion on land. *Journal of Experimental Biology* 83:3325–3332.
- Ghigliazza, R.M., Altendorfer, R., Holmes, P., and Koditschek, D.E. 2003. A simply stabilized running model. *SIAM Journal on Applied Dynamical Systems* 2(2):187–218.
- McGeer, T. 1990. Passive dynamic walking. *International Journal of Robotics Research* 9(2):62–82.
- Nakanishi, J., Fukuda, T., and Koditschek, D.E. 2000.
 A brachiating robot controller. *IEEE Transactions on Robotics and Automation* 16(2):109–123.
- Rizzi, A., Whitcomb, L.L., and Koditschek, D.E. 1992. Distributed real-time control of a spatial robot juggler. *IEEE Computer* 25(5):12–24.
- Saranli, U. 2000. SimSect hybrid dynamical simulation environment. Technical Report CSE-TR-437-00, University of Michigan.
- Saranli, U. 2002. Dynamic Locomotion with a Hexapod Robot. PhD thesis, University of Michigan at Ann Arbor.
- Saranli, U., Buehler, M., and Koditschek, D.E. 2001. RHex: a simple and highly mobile hexapod robot. *International Journal of Robotics Research* 20(7):616–631.
- Schmitt, J., and Holmes, P. 2003. Mechanical models for insect locomotion: active muscles and energy losses. *Biological Cybernetics* 89:43–55.
- Schwind, W.J. 1998. Spring Loaded Inverted Pendulum Running: A Plant Model. PhD thesis, University of Michigan at Ann Arbor.
- Seyfarth, A., and Geyer, H. 2002. Natural control of springlike running – optimized self-stabilization. *Proceedings of* the 5th International Conference on Climbing and Walking Robots (CLAWAR 2002), Paris, France, pp. 81–85.
- Seyfarth, A., Geyer, H., Günther, M., and Blickhan, R. 2002. A movement criterion for running. *Journal of Biomechanics* 35:649–655.
- Seyfarth, A., Geyer, H., and Herr, H. 2003. Swing-leg retraction: a simple control model for stable running. *Journal of Experimental Biology* 206:2547–2555.
- Weingarten, J.D., Lopes, G.A.D., Buehler, M., Groff, R.E., and Koditschek, D.E. 2004. Automated gait adaptation for legged robots. *Proceedings of the International Conference on Robotics and Automation (ICRA)*, New Orleans, LA, Vol. 3, pp. 2153–2158.
- Westervelt, E.R., Grizzle, J.W., and Koditschek, D.E. 2003. Hybrid zero dynamics of planar biped walkers. *IEEE Transactions on Automatic Control* 48(1):42–56.